Eur. Phys. J. C 6, 385–401 (1999)
DOI 10.1007/s100529801043

THE EUROPEAN PHYSICAL JOURNAL C


# Search for scalar fermions and long-lived scalar leptons at centre-of-mass energies of 130 GeV to 172 GeV

DELPHI Collaboration

P. Abreu[21], W. Adam[50], T. Adye[36], P. Adzic[11], I. Ajinenko[42], G.D. Alekseev[16], R. Alemany[49], P.P. Allport[22], S. Almehed[24], U. Amaldi[9], S. Amato[47], E.G. Anassontzis[3], P. Andersson[44], A. Andreazza[9], S. Andringa[21], P. Antilogus[25], W-D. Apel[17], Y. Arnoud[14], B. Åsman[44], J-E. Augustin[25], A. Augustinus[9], P. Baillon[9], P. Bambade[19], F. Barao[21], G. Barbiellini[46], R. Barbier[25], D.Y. Bardin[16], G. Barker[9], A. Baroncelli[38], M. Battaglia[15], M. Baubillier[23], K-H. Becks[52], M. Begalli[6], P. Beilliere[8], Yu. Belokopytov[9,53], A.C. Benvenuti[5], C. Berat[14], M. Berggren[25], D. Bertini[25], D. Bertrand[2], M. Besancon[39], F. Bianchi[45], M. Bigi[45], M.S. Bilenky[16], M-A. Bizouard[19], D. Bloch[10], H.M. Blom[30], M. Bonesini[27], W. Bonivento[27], M. Boonekamp[39], P.S.L. Booth[22], A.W. Borgland[4], G. Borisov[19], C. Bosio[41], O. Botner[48], E. Boudinov[30], B. Bouquet[19], C. Bourdarios[19], T.J.V. Bowcock[22], I. Boyko[16], I. Bozovic[11], M. Bozzo[13], P. Branchini[38], T. Brenke[52], R.A. Brenner[48], P. Bruckman[18], J-M. Brunet[8], L. Bugge[32], T. Buran[32], T. Burgsmueller[52], P. Buschmann[52], S. Cabrera[49], M. Caccia[27], M. Calvi[27], A.J. Camacho Rozas[40], T. Camporesi[9], V. Canale[37], F. Carena[9], L. Carroll[22], C. Caso[13], M.V. Castillo Gimenez[49], A. Cattai[9], Ch. Cerruti[10], V. Chabaud[9], Ph. Charpentier[9], L. Chaussard[25], P. Checchia[35], G.A. Chelkov[16], R. Chierici[45], P. Chliapnikov[42], P. Chochula[7], V. Chorowicz[25], J. Chudoba[29], P. Collins[9], M. Colomer[49], R. Contri[13], E. Cortina[49], G. Cosme[19], F. Cossutti[39], J-H. Cowell[22], H.B. Crawley[1], D. Crennell[36], G. Crosetti[13], J. Cuevas Maestro[33], S. Czellar[15], G. Damgaard[28], M. Davenport[9], W. Da Silva[23], A. Deghorain[2], G. Della Ricca[46], P. Delpierre[26], N. Demaria[9], A. De Angelis[9], W. De Boer[17], S. De Brabandere[2], C. De Clercq[2], B. De Lotto[46], A. De Min[35], L. De Paula[47], H. Dijkstra[9], L. Di Ciaccio[37], A. Di Diodato[37], J. Dolbeau[8], K. Doroba[51], M. Dracos[10], J. Drees[52], M. Dris[31], A. Duperrin[25], J-D. Durand[25,9], R. Ehret[17], G. Eigen[4], T. Ekelof[48], G. Ekspong[44], M. Ellert[48], M. Elsing[9], J-P. Engel[10], B. Erzen[43], M. Espirito Santo[21], E. Falk[24], G. Fanourakis[11], D. Fassouliotis[11], J. Fayot[23], M. Feindt[17], P. Ferrari[27], A. Ferrer[49], E. Ferrer-Ribas[19], S. Fichet[23], A. Firestone[1], P.-A. Fischer[9], U. Flagmeyer[52], H. Foeth[9], E. Fokitis[31], F. Fontanelli[13], B. Franek[36], A.G. Frodesen[4], R. Fruhwirth[50], F. Fulda-Quenzer[19], J. Fuster[49], A. Galloni[22], D. Gamba[45], S. Gamblin[19], M. Gandelman[47], C. Garcia[49], J. Garcia[40], C. Gaspar[9], M. Gaspar[47], U. Gasparini[35], Ph. Gavillet[9], E.N. Gazis[31], D. Gele[10], J-P. Gerber[10], N. Ghodbane[25], I. Gil[49], F. Glege[52], R. Gokieli[51], B. Golob[43], P. Goncalves[21], I. Gonzalez Caballero[40], G. Gopal[36], L. Gorn[1,54], M. Gorski[51], Yu. Gouz[42], V. Gracco[13], J. Grahl[1], E. Graziani[38], C. Green[22], P. Gris[39], K. Grzelak[51], M. Gunther[48], J. Guy[36], F. Hahn[9], S. Hahn[52], S. Haider[9], A. Hallgren[48], K. Hamacher[52], F.J. Harris[34], V. Hedberg[24], S. Heising[17], J.J. Hernandez[49], P. Herquet[2], H. Herr[9], T.L. Hessing[34], J.-M. Heuser[52], E. Higon[49], S-O. Holmgren[44], P.J. Holt[34], D. Holthuizen[30], S. Hoorelbeke[2], M. Houlden[22], J. Hrubec[50], K. Huet[2], K. Hultqvist[44], J.N. Jackson[22], R. Jacobsson[9], P. Jalocha[9], R. Janik[7], Ch. Jarlskog[24], G. Jarlskog[24], P. Jarry[39], B. Jean-Marie[19], E.K. Johansson[44], P. Jonsson[24], C. Joram[9], P. Juillot[10], F. Kapusta[23], K. Karafasoulis[11], S. Katsanevas[25], E.C. Katsoufis[31], R. Keranen[17], B.A. Khomenko[16], N.N. Khovanski[16], A. Kiiskinen[15], B. King[22], N.J. Kjaer[30], O. Klapp[52], H. Klein[9], P. Kluit[30], D. Knoblauch[17], P. Kokkinias[11], A. Konopliannikov[42], M. Koratzinos[9], V. Kostioukhine[42], C. Kourkoumelis[3], O. Kouznetsov[16], M. Krammer[50], C. Kreuter[9], E. Kriznic[43], J. Krstic[11], Z. Krumstein[16], P. Kubinec[7], W. Kucewicz[18], K. Kurvinen[15], J.W. Lamsa[1], D.W. Lane[1], P. Langefeld[52], V. Lapin[42], J-P. Laugier[39], R. Lauhakangas[15], G. Leder[50], F. Ledroit[14], V. Lefebure[2], L. Leinonen[44], A. Leisos[11], R. Leitner[29], G. Lenzen[52], V. Lepeltier[19], T. Lesiak[18], M. Lethuillier[39], J. Libby[34], D. Liko[9], A. Lipniacka[44], I. Lippi[35], B. Loerstad[24], M. Lokajicek[12], J.G. Loken[34], J.H. Lopes[47], J.M. Lopez[40], R. Lopez-Fernandez[14], D. Loukas[11], P. Lutz[39], L. Lyons[34], J. MacNaughton[50], J.R. Mahon[6], A. Maio[21], A. Malek[52], T.G.M. Malmgren[44], V. Malychev[16], F. Mandl[50], J. Marco[40], R. Marco[40], B. Marechal[47], M. Margoni[35], J-C. Marin[9], C. Mariotti[9], A. Markou[11], C. Martinez-Rivero[19], F. Martinez-Vidal[49], S. Marti i Garcia[22], N. Mastroyiannopoulos[11], F. Matorras[40], C. Matteuzzi[27], G. Matthiae[37], J. Mazik[29], F. Mazzucato[35], M. Mazzucato[35], M. Mc Cubbin[22], R. Mc Kay[1], R. Mc Nulty[9], G. Mc Pherson[22], C. Meroni[27], W.T. Meyer[1], A. Miagkov[42], E. Migliore[45], L. Mirabito[25], U. Mjoernmark[24], T. Moa[44], R. Moeller[28], K. Moenig[9], M.R. Monge[13], X. Moreau[23], P. Morettini[13], G. Morton[34], U. Mueller[52], K. Muenich[52], M. Mulders[30], C. Mulet-Marquis[14], R. Muresan[24], W.J. Murray[36], B. Muryn[14,18], G. Myatt[34], T. Myklebust[32], F. Naraghi[14], S. Navas[49], K. Nawrocki[51], P. Negri[27], N. Neufeld[9], N. Neumeister[50], R. Nicolaidou[14], B.S. Nielsen[28], V. Nikolaenko[10], M. Nikolenko[10,16], V. Nomokonov[15], A. Normand[22], A. Nygren[24], V. Obraztsov[42], A.G. Olshevski[16], A. Onofre[21], R. Orava[15], G. Orazi[10], K. Osterberg[15], A. Ouraou[39], M. Paganoni[27], S. Paiano[5], R. Pain[23], R. Paiva[21], J. Palacios[34], H. Palka[18], Th.D. Papadopoulou[31], K. Papageorgiou[11], L. Pape[9],

C. Parkes[34], F. Parodi[13], U. Parzefall[22], A. Passeri[38], O. Passon[52], M. Pegoraro[35], L. Peralta[21], M. Pernicka[50], A. Perrotta[5], C. Petridou[46], A. Petrolini[13], H.T. Phillips[36], G. Piana[13], F. Pierre[39], M. Pimenta[21], E. Piotto[27], T. Podobnik[43], M.E. Pol[6], G. Polok[18], P. Poropat[46], V. Pozdniakov[16], P. Privitera[37], N. Pukhaeva[16], A. Pullia[27], D. Radojicic[34], S. Ragazzi[27], H. Rahmani[31], D. Rakoczy[50], P.N. Ratoff[20], A.L. Read[32], P. Rebecchi[9], N.G. Redaelli[27], M. Regler[50], D. Reid[9], R. Reinhardt[52], P.B. Renton[34], L.K. Resvanis[3], F. Richard[19], J. Ridky[12], G. Rinaudo[45], O. Rohne[32], A. Romero[45], P. Ronchese[35], E.I. Rosenberg[1], P. Rosinsky[7], P. Roudeau[19], T. Rovelli[5], V. Ruhlmann-Kleider[39], A. Ruiz[40], H. Saarikko[15], Y. Sacquin[39], A. Sadovsky[16], G. Sajot[14], J. Salt[49], D. Sampsonidis[11], M. Sannino[13], H. Schneider[17], Ph. Schwemling[23], U. Schwickerath[17], M.A.E. Schyns[52], F. Scuri[46], P. Seager[20], Y. Sedykh[16], A.M. Segar[34], R. Sekulin[36], R.C. Shellard[6], A. Sheridan[22], M. Siebel[52], R. Silvestre[39], L. Simard[39], F. Simonetto[35], A.N. Sisakian[16], T.B. Skaali[32], G. Smadja[25], N. Smirnov[42], O. Smirnova[24], G.R. Smith[36], A. Sopczak[17], R. Sosnowski[51], T. Spassov[21], E. Spiriti[38], P. Sponholz[52], S. Squarcia[13], D. Stampfer[50], C. Stanescu[38], S. Stanic[43], S. Stapnes[32], K. Stevenson[34], A. Stocchi[19], J. Strauss[50], R. Strub[10], B. Stugu[4], M. Szczekowski[51], M. Szeptycka[51], T. Tabarelli[27], O. Tchikilev[42], F. Tegenfeldt[48], F. Terranova[27], J. Thomas[34], A. Tilquin[26], J. Timmermans[30], L.G. Tkatchev[16], T. Todorov[10], S. Todorova[10], D.Z. Toet[30], A. Tomaradze[2], B. Tome[21], A. Tonazzo[27], L. Tortora[38], G. Transtromer[24], D. Treille[9], G. Tristram[8], C. Troncon[27], A. Tsirou[9], M-L. Turluer[39], I.A. Tyapkin[16], S. Tzamarias[11], B. Ueberschaer[52], O. Ullaland[9], V. Uvarov[42], G. Valenti[5], E. Vallazza[46], C. Vander Velde[2], G.W. Van Apeldoorn[30], P. Van Dam[30], J. Van Eldik[30], A. Van Lysebetten[2], I. Van Vulpen[30], N. Vassilopoulos[34], G. Vegni[27], L. Ventura[35], W. Venus[36], F. Verbeure[2], M. Verlato[35], L.S. Vertogradov[16], V. Verzi[37], D. Vilanova[39], L. Vitale[46], E. Vlasov[42], A.S. Vodopyanov[16], G. Voulgaris[3], V. Vrba[12], H. Wahlen[52], C. Walck[44], C. Weiser[17], D. Wicke[52], J.H. Wickens[2], G.R. Wilkinson[9], M. Winter[10], M. Witek[18], G. Wolf[9], J. Yi[1], O. Yushchenko[42], A. Zalewska[18], P. Zalewski[51], D. Zavrtanik[43], E. Zevgolatakos[11], N.I. Zimin[16,24], G.C. Zucchelli[44], G. Zumerle[35]

[1] Department of Physics and Astronomy, Iowa State University, Ames IA 50011-3160, USA
[2] Physics Department, Univ. Instelling Antwerpen, Universiteitsplein 1, BE-2610 Wilrijk, Belgium and IIHE, ULB-VUB, Pleinlaan 2, BE-1050 Brussels, Belgium and Faculté des Sciences, Univ. de l'Etat Mons, Av. Maistriau 19, BE-7000 Mons, Belgium
[3] Physics Laboratory, University of Athens, Solonos Str. 104, GR-10680 Athens, Greece
[4] Department of Physics, University of Bergen, Allégaten 55, NO-5007 Bergen, Norway
[5] Dipartimento di Fisica, Università di Bologna and INFN, Via Irnerio 46, I-40126 Bologna, Italy
[6] Centro Brasileiro de Pesquisas Físicas, rua Xavier Sigaud 150, BR-22290 Rio de Janeiro, Brazil and Depto. de Física, Pont. Univ. Católica, C.P. 38071 BR-22453 Rio de Janeiro, Brazil and Inst. de Física, Univ. Estadual do Rio de Janeiro, rua São Francisco Xavier 524, Rio de Janeiro, Brazil
[7] Comenius University, Faculty of Mathematics and Physics, Mlynska Dolina, SK-84215 Bratislava, Slovakia
[8] Collège de France, Lab. de Physique Corpusculaire, IN2P3-CNRS, FR-75231 Paris Cedex 05, France
[9] CERN, CH-1211 Geneva 23, Switzerland
[10] Institut de Recherches Subatomiques, IN2P3 - CNRS/ULP - BP20, F-67037 Strasbourg Cedex, France
[11] Institute of Nuclear Physics, N.C.S.R. Demokritos, P.O. Box 60228, GR-15310 Athens, Greece
[12] FZU, Inst. of Phys. of the C.A.S. High Energy Physics Division, Na Slovance 2, CZ-180 40, Praha 8, Czech Republic
[13] Dipartimento di Fisica, Università di Genova and INFN, Via Dodecaneso 33, I-16146 Genova, Italy
[14] Institut des Sciences Nucléaires, IN2P3-CNRS, Université de Grenoble 1, F-38026 Grenoble Cedex, France
[15] Helsinki Institute of Physics, HIP, P.O. Box 9, FI-00014 Helsinki, Finland
[16] Joint Institute for Nuclear Research, Dubna, Head Post Office, P.O. Box 79, RU-101 000 Moscow, Russian Federation
[17] Institut für Experimentelle Kernphysik, Universität Karlsruhe, Postfach 6980, D-76128 Karlsruhe, Germany
[18] Institute of Nuclear Physics and University of Mining and Metalurgy, Ul. Kawiory 26a, PL-30055 Krakow, Poland
[19] Université de Paris-Sud, Lab. de l'Accélérateur Linéaire, IN2P3-CNRS, Bât. 200, FR-91405 Orsay Cedex, France
[20] School of Physics and Chemistry, University of Lancaster, Lancaster LA1 4YB, UK
[21] LIP, IST, FCUL - Av. Elias Garcia, 14-1°, PT-1000 Lisboa Codex, Portugal
[22] Department of Physics, University of Liverpool, P.O. Box 147, Liverpool L69 3BX, UK
[23] LPNHE, IN2P3-CNRS, Univ. Paris VI et VII, Tour 33 (RdC), 4 place Jussieu, F-75252 Paris Cedex 05, France
[24] Department of Physics, University of Lund, Sölvegatan 14, SE-223 63 Lund, Sweden
[25] Université Claude Bernard de Lyon, IPNL, IN2P3-CNRS, F-69622 Villeurbanne Cedex, France
[26] Univ. d'Aix - Marseille II - CPP, IN2P3-CNRS, F-13288 Marseille Cedex 09, France
[27] Dipartimento di Fisica, Università di Milano and INFN, Via Celoria 16, I-20133 Milan, Italy
[28] Niels Bohr Institute, Blegdamsvej 17, DK-2100 Copenhagen Ø, Denmark
[29] NC, Nuclear Centre of MFF, Charles University, Areal MFF, V Holesovickach 2, CZ-180 00, Praha 8, Czech Republic
[30] NIKHEF, Postbus 41882, NL-1009 DB Amsterdam, The Netherlands
[31] National Technical University, Physics Department, Zografou Campus, GR-15773 Athens, Greece
[32] Physics Department, University of Oslo, Blindern, NO-1000 Oslo 3, Norway
[33] Dpto. Fisica, Univ. Oviedo, Avda. Calvo Sotelo s/n, E-33007 Oviedo, Spain
[34] Department of Physics, University of Oxford, Keble Road, Oxford OX1 3RH, UK
[35] Dipartimento di Fisica, Università di Padova and INFN, Via Marzolo 8, I-35131 Padua, Italy
[36] Rutherford Appleton Laboratory, Chilton, Didcot OX11 OQX, UK

[37] Dipartimento di Fisica, Università di Roma II and INFN, Tor Vergata, I-00173 Rome, Italy
[38] Dipartimento di Fisica, Università di Roma III and INFN, Via della Vasca Navale 84, I-00146 Rome, Italy
[39] DAPNIA/Service de Physique des Particules, CEA-Saclay, F-91191 Gif-sur-Yvette Cedex, France
[40] Instituto de Fisica de Cantabria (CSIC-UC), Avda. los Castros s/n, E-39006 Santander, Spain
[41] Dipartimento di Fisica, Università degli Studi di Roma La Sapienza, Piazzale Aldo Moro 2, I-00185 Rome, Italy
[42] Inst. for High Energy Physics, Serpukov P.O. Box 35, Protvino, (Moscow Region), Russian Federation
[43] J. Stefan Institute, Jamova 39, SI-1000 Ljubljana, Slovenia and Department of Astroparticle Physics, School of Environmental Sciences, Kostanjeviska 16a, Nova Gorica, SI-5000 Slovenia, and Department of Physics, University of Ljubljana, SI-1000 Ljubljana, Slovenia
[44] Fysikum, Stockholm University, Box 6730, SE-113 85 Stockholm, Sweden
[45] Dipartimento di Fisica Sperimentale, Università di Torino and INFN, Via P. Giuria 1, I-10125 Turin, Italy
[46] Dipartimento di Fisica, Università di Trieste and INFN, Via A. Valerio 2, I-34127 Trieste, Italy and Istituto di Fisica, Università di Udine, I-33100 Udine, Italy
[47] Univ. Federal do Rio de Janeiro, C.P. 68528 Cidade Univ., Ilha do Fundão BR-21945-970 Rio de Janeiro, Brazil
[48] Department of Radiation Sciences, University of Uppsala, P.O. Box 535, SE-751 21 Uppsala, Sweden
[49] IFIC, Valencia-CSIC, and D.F.A.M.N., U. de Valencia, Avda. Dr. Moliner 50, E-46100 Burjassot (Valencia), Spain
[50] Institut für Hochenergiephysik, Österr. Akad. d. Wissensch., Nikolsdorfergasse 18, A-1050 Vienna, Austria
[51] Inst. Nuclear Studies and University of Warsaw, Ul. Hoza 69, PL-00681 Warsaw, Poland
[52] Fachbereich Physik, University of Wuppertal, Postfach 100 127, D-42097 Wuppertal, Germany
[53] On leave of absence from IHEP Serpukhov
[54] Now at University of Florida

Received: 13 July 1998 / Published online: 19 November 1998

**Abstract.** Data taken by DELPHI during the 1995 and 1996 LEP runs have been used to search for the supersymmetric partners of electron, muon and tau leptons and of top and bottom quarks. The observations are in agreement with standard model predictions. Limits are set on sfermion masses. Searches for long lived scalar leptons from low scale supersymmetry breaking models exclude stau masses below 55 GeV/$c^2$ at the 95% confidence level, irrespective of the gravitino mass.

## 1 Introduction

During the 1996 data taking period the LEP accelerator operated for the first time at centre-of-mass energies above the WW production threshold. This increase in energy allowed new searches for scalar partners of leptons (sleptons) and quarks (squarks), which are predicted by supersymmetric (SUSY) models and, in particular, the minimal supersymmetric extension of the standard model (MSSM) [1]. Limits on the production of these particles have already been published, based on data taken at 130GeVand above [2,3]. This paper reports on a search for these particles in data taken by DELPHI at centre-of-mass energies of 161 and 172 GeV. In the calculation of limits, these results have been combined with already published ones [2] at intermediate energies of 130–136 GeV. For the search for scalar taus, the analysis of data taken at all these energies is presented in this paper.

Assuming R-parity conservation[1], the decay chain of sfermions will end with a stable particle, the lightest supersymmetric particle (LSP). Cosmological constraints suggest that the LSP is neutral. Since this particle is expected to be undetectable by DELPHI, the events will be characterised by missing momentum and energy. The lightest neutralino, $\tilde{\chi}_1^0$, is commonly assumed to be the LSP but cases where the LSP is a light gravitino, $\tilde{G}$ , will also be considered. Production cross-sections of sfermions depend on the mass of supersymmetric particles and the MSSM parameters (the supersymmetry-conserving mass parameter, $\mu$, the soft supersymmetry breaking term associated to the $SU(2)_L$ group, $M_2$, and the ratio of the vacuum expectation values of the two Higgs doublets, $\tan\beta$). In this study, the unification condition $M_1 = \frac{5}{3}\tan^2\theta_W M_2$, where $M_1$ is the soft supersymmetry breaking parameter associated with the $U(1)_Y$ group, is assumed to be valid.

The search for the supersymmetric partners of the top quark (often called stop) is motivated by the prediction of a low mass due to the large top quark Yukawa coupling. Furthermore a large mass difference between the two physical stop-states is possible, resulting from mixing right- ($\tilde{t}_R$) and left-handed ($\tilde{t}_L$) components. The size of the mass splitting is also related to the high mass of the top quark [4]. As a consequence, for $\tan\beta \lesssim 10$, the lighter of the two physical states ($\tilde{t}_1$) could be the lightest charged supersymmetric particle. Within the MSSM, stop/anti-stop pairs could be produced via the s-channel exchange of a $Z^0$ or $\gamma$, resulting in events with two jets and missing momentum. In this paper the decay of stop into $c\tilde{\chi}_1^0$ is investigated. Similar arguments apply for sbottom. Due to the lower mass of the b quark, strong effects of $\tilde{b}_R$-$\tilde{b}_L$ mixing are only expected for values of $\tan\beta \gtrsim 10$ when the decay into $b\tilde{\chi}_1^0$ is considered. The topology of these events closely resembles that for stop decays. The search for squark states is presented in Sect. 4.

The production of sleptons can also proceed via $e^+e^-$ annihilation into $Z^0/\gamma$. For smuons and selectrons, no sig-

[1] We do not consider R-Parity violating processes in this paper.

nificant mixing of right- and left-handed states is expected due to the small masses of electrons and muons. For selectrons, however, t-channel diagrams involving a neutralino can contribute and generate $\tilde{e}_R\tilde{e}_L$ final states. Within the MSSM, sleptons are pair-produced and may decay (1) to the corresponding lepton and the lightest neutralino, or (2) to the corresponding neutrino and the lightest chargino, or (3) to the lepton and the second lightest neutralino. In most of the parameter-space, only (1) occurs. The decay mode (2) can be present if $\mu \gtrsim 110$ GeV/$c^2$ and the mass of the lightest neutralino is below about 40 GeV/$c^2$. At higher neutralino masses, the chargino is too massive to be produced in the decay of a slepton with mass below about 65 GeV/$c^2$. However, the ($\mu$,$M_2$) combinations that yield such low neutralino masses at $\mu \gtrsim 110$ GeV/$c^2$ have already been excluded by previous searches [5,6]. The decay mode (3) can occur if $\mu \sim -90$ GeV/$c^2$ and $\tan\beta$ is less than about 5. While this decay mode is kinematically accessible in some cases, the MSSM predicts that its branching ratio is too small to be observed in this experiment. Hence (2) and (3) have been neglected and the slepton analysis has been designed to be sensitive to (1), where sleptons undergo a two-body decay into a lepton and an undetected neutralino. This analysis is described in Sect. 5.

In addition to the "standard" search for scalar leptons, a search for long lived scalar leptons has been performed using data collected at centre-of-mass energies of 130-136, 161 and 172 GeV. This was motivated by low scale supersymmetry breaking models such as the gauge mediated SUSY breaking models [7–11], where the lightest supersymmetric particle is the gravitino ($\tilde{G}$ ), while the next to lightest supersymmetric particle (NLSP) could be a right-handed slepton. This analysis is described in Sect. 6.

## 2 Detector description

The DELPHI detector and its performance have been described in detail elsewhere [12,13]; only those components relevant for the present analyses are discussed here.

Charged particle tracks were reconstructed in the 1.2 T solenoidal magnetic field by a system of cylindrical tracking chambers. These were the Microvertex Detector (VD), the Inner Detector (ID), the Time Projection Chamber (TPC) and the Outer Detector (OD). In addition, two planes of drift chambers aligned perpendicular to the beam axis (Forward Chambers A and B) tracked particles in the forward and backward directions, covering polar angles $11° < \theta < 33°$ and $147° < \theta < 169°$ with respect to the beam ($z$) direction.

The VD consisted of three cylindrical layers of silicon detectors, at radii 6.3 cm, 9.0 cm and 11.0 cm. All three layers measured coordinates in the $xy$ plane, transverse to the beam. The closest (6.3 cm) and the outer (11.0 cm) layers contained double-sided detectors to also measure $z$ coordinates. In 1996 the polar angle coverage of the VD was from 24° to 156° and detectors were added to the inner layer providing a further measurement of the $z$ coordinate. The ID was a cylindrical drift chamber (inner radius 12 cm and outer radius 22 cm) covering polar angles between 15° and 165°. The TPC, the principal tracking device of DELPHI, was a cylinder of 30 cm inner radius, 122 cm outer radius and had a length of 2.7 m. Each end-plate was divided into 6 sectors, with 192 sense wires used for the dE/dx measurement and 16 circular pad rows used for 3 dimensional space-point reconstruction. The OD consisted of 5 layers of drift cells at radii between 192 cm and 208 cm, covering polar angles between 43° and 137°.

The average momentum resolution for the charged particles in hadronic final states was in the range $\Delta p/p^2 \simeq 0.001$ to $0.01(\mathrm{GeV}/c)^{-1}$, depending on which detectors were used in the track fit [13].

The electromagnetic calorimeters were the High density Projection Chamber (HPC) covering the barrel region of $40° < \theta < 140°$, the Forward ElectroMagnetic Calorimeter (FEMC) covering $11° < \theta < 36°$ and $144° < \theta < 169°$, and the STIC, a Scintillator TIle Calorimeter which extended coverage down to 1.66° from the beam axis in both directions. The 40° taggers were a series of single layer scintillator-lead counters used to veto electromagnetic particles that would otherwise have been missed in the region between the HPC and FEMC. The efficiency to register a photon with energy above 5 GeV at polar angles between 20° and 160°, measured with the LEP1 data, was above 99% [14]. The hadron calorimeter (HCAL) covered 98% of the solid angle. Muons with momenta above 2 GeV/c penetrated the HCAL and were recorded in a set of Muon Drift Chambers.

## 3 Data samples, event generators and limits

Integrated luminosities of 5.9 pb$^{-1}$, 9.6 pb$^{-1}$, 0.7 pb$^{-1}$ and 9.5 pb$^{-1}$ were accumulated at centre-of-mass energies of 130-136 GeV, 161 GeV, 170 GeV and 172 GeV respectively.

Simulated events were generated with several different programs in order to evaluate signal efficiency and background contamination. All the models used JETSET 7.4 [15] for quark fragmentation with parameters tuned to represent DELPHI data [16].

The program SUSYGEN [17] was used to generate slepton events and to calculate cross-sections and branching ratios. It was verified that the result obtained agreed with the calculations of reference [18]. Stop and sbottom events were generated according to the expected differential cross-sections, using the BASES and SPRING program packages [19]. Special care was taken in the modelling of the stop hadronisation [20].

The background processes $e^+e^- \to q\bar{q}(n\gamma)$ and processes leading to four-fermion final states, $(Z^0/\gamma)^*(Z^0/\gamma)^*$, $W^{+*}W^{-*}$, $We\nu_e$, and $Z^0e^+e^-$ were generated using PYTHIA [15]. The cut on the invariant mass of the virtual $(Z^0/\gamma)^*$ in the $(Z^0/\gamma)^*(Z^0/\gamma)^*$ process was set at 2 GeV/$c^2$, in order to determine the background from low mass $f\bar{f}$ pairs. The calculation of the four-fermion background was verified using the program EXCALIBUR [21],

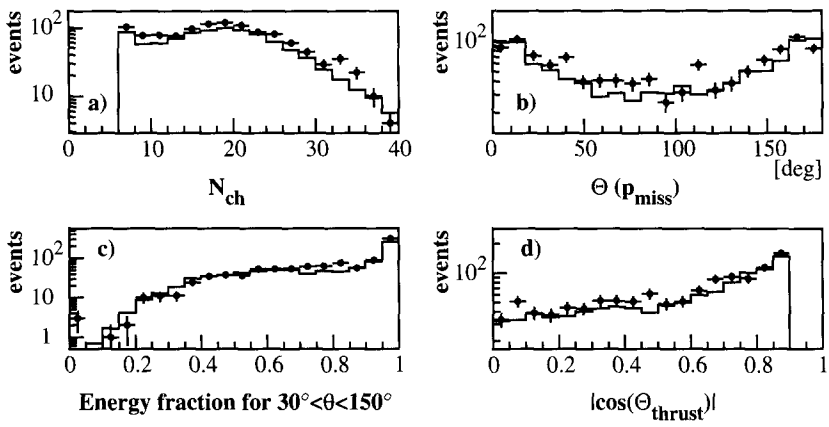


**Fig. 1a–d.** Distribution of key event variables used in the preselection of the squark analyses for 161 GeV data (points) and SM background simulation (lines). The distributions are shown after the selections on charged multiplicity, $N_{ch}$, polar angle of the thrust axis, $\theta_{thrust}$, and missing transverse momentum

which consistently takes into account all amplitudes leading to a given four-fermion final state. The version of EXCALIBUR used did not, however, include the transverse momentum of initial state radiation. Two-photon interactions leading to hadronic final states were simulated using TWOGAM [22] and BDKRC [23] for the Quark Parton Model contribution. Leptonic final states with muons and taus were also modelled with BDKRC. BDK [23] was used for final states with electrons only.

Generated signal and background events were passed through detailed detector response simulation [13] and processed with the same reconstruction and analysis programs as the real data. The number of background events simulated was mostly several times larger than the number expected in the real data.

The likelihood ratio method described in [24] was used for the calculation of exclusion zones, combining the results from different centre-of-mass energies. It provides an optimal combination for each mass taking into account the expected levels of background and signal and the number of candidates. Expected exclusion zones were calculated using the same algorithm, from simulated background-only experiments.

## 4 Scalar quark decay into neutralino and quark

Stop and sbottom have been searched for in the decay modes $c\tilde{\chi}_1^0$ and $b\tilde{\chi}_1^0$, respectively. In both cases the experimental signatures consist of events with two jets and missing momentum taken by the two undetected $\tilde{\chi}_1^0$. Consequently the analyses for the two flavours showed many similarities. Since event parameters such as visible energy depend highly on the mass difference $\Delta M$ between squark and LSP, selection procedures were optimised separately for the degenerate ($\Delta M \leq 10$ GeV/$c^2$) and non-degenerate ($\Delta M > 10$ GeV/$c^2$) cases. The main differences between stop and sbottom events arise from the hadronisation, assumed to occur either before ($\tilde{t}$) or after ($\tilde{b}$) the decay of the scalar quark. These differences are visible in particular in the degenerate case. Consequently different initial selections were used at the preselection level for the stop and sbottom analyses at low $\Delta M$.

### 4.1 Selection of candidates

Events were preselected by a filter of sequential cuts. The filter selected hadronic events and was aimed at rejecting the main sources of background in each of the domains: WW and $Z^0\gamma$ for the non degenerate case, and events from $\gamma\gamma$ processes for the degenerate case. Reconstructed charged particles were required to have momentum above 100 MeV/$c$ and impact parameters below 4 cm in the transverse plane and below 10 cm in the longitudinal direction. Clusters in the calorimeters were interpreted as neutral particles if they were not associated to charged particles and their energy exceeded 100 MeV. Jets were reconstructed using the JADE [25] algorithm with $y_{min} = 0.9$ to force the events into two jets. Decays of b-quarks were tagged using a probabilistic method based on the impact parameters of tracks with respect to the main vertex [13]. The variable $P_E^+$ used in this analysis was the probability for tracks with a positive impact parameter to be compatible with the main vertex, the impact parameter sign being defined by the jet direction.

All events were required to be well contained in the well-instrumented region by requiring the cosine of the thrust direction to be in the range −0.9 to 0.9. Events caused by synchrotron radiation and off-momentum beam particles, characterised by tracks seen only in the innermost detectors VD and ID, were rejected. The total energy in the electromagnetic calorimeters was required to be less than 50 GeV to reject events from Bhabha scattering. The momentum of the leading charged particle had to be above 1 GeV/$c$. In addition, at a centre-of-mass energy of 172 GeV, the total transverse energy in the event had to exceed 5 GeV and the transverse energy of the charged particles in the highest energy jet to exceed 1 GeV. These selections removed soft events from $\gamma\gamma$ processes.

For the degenerate case ($\Delta M \leq 10$ GeV/$c^2$), events had to contain at least 5 charged particles for the stop and 7 for the sbottom selection. The total energy had to be in the range 5 to 40 GeV, with a visible mass (in GeV/$c^2$) exceeding 40% of this energy value. A missing transverse momentum of at least 3 GeV/$c$ (2 GeV/$c$) was required for the stop (sbottom) selection. Events in the very forward and backward regions were rejected by requiring the fraction of the visible energy in a 30° cone around the

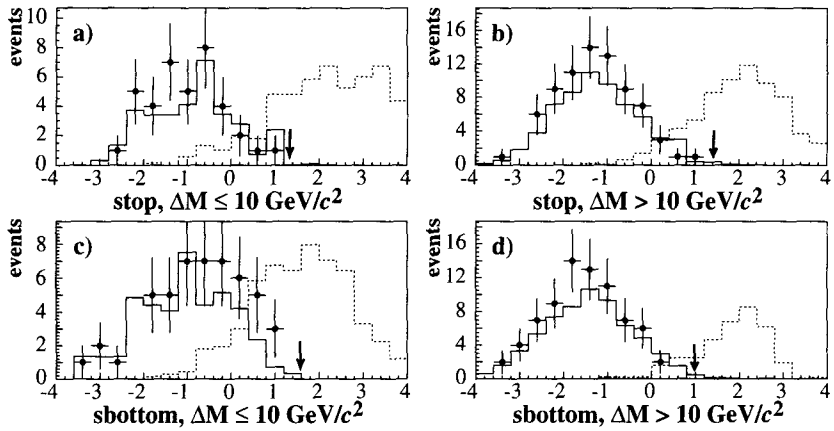


**Fig. 2.** Distributions of the discriminating functions used in the second step of the search for stop **a,b** and sbottom **c,d** particles at $\sqrt{s} =$ 172 GeV. **a** and **c** correspond to the degenerate case, **b** and **d** to the non-degenerate case. Dots with error bars indicate the distributions for data, full lines the SM background simulation, and the dashed lines the expectation for a 60 GeV/$c^2$ **a,c** or 80 GeV/$c^2$ **b,d** squark, respectively, at an LSP mass of 50 GeV/$c^2$. The arrows indicate the cut values chosen in order to retain about one background event

**Table 1.** Coefficients of the discriminating functions optimised for two mass domains in the stop and sbottom searches at $\sqrt{s} = 161$ GeV. Jets are numbered according to their energy, $\delta\phi_{jets}$ indicates the angle between the two jets in the transverse plane

| | stop | | sbottom | |
|---|---|---|---|---|
| $\Delta M$ (GeV/$c^2$) | $\leq 10$ | $> 10$ | $\leq 10$ | $> 10$ |
| Charged multiplicity | - | - | 0.20 | - |
| Visible mass (GeV/$c^2$) | - | -0.02 | - | 0.03 |
| $E$ (charged particles, in GeV) | 0.20 | 0.02 | - | - |
| $E$ (at $> 30°$ from beam axis, in GeV) | 7.26 | 1.92 | - | - |
| Missing transverse momentum (GeV/$c$) | 0.23 | - | - | 0.03 |
| $3^{rd}$ Fox-Wolfram moment [27] | 1.51 | 0.99 | - | - |
| acollinearity (degree) | - | -0.03 | - | -0.03 |
| acoplanarity (degree) | - | 0.03 | 0.01 | 0.03 |
| thrust | - | -4.25 | - | - |
| $\lvert\cos(\theta_{thrust})\rvert$ | -1.21 | - | -1.54 | -1.16 |
| b-tagging probability ($P_E^+$) | -0.66 | - | - | -1.42 |
| $M$ (jet 1, in GeV/$c^2$) | - | 0.06 | - | -0.04 |
| $p$ (jet 1, in GeV/$c$) | -0.23 | - | - | - |
| Charged multiplicity (jet 2) | -0.09 | - | - | - |
| $M$ (jet 2, in GeV/$c^2$) | - | -0.05 | - | -0.46 |
| $E$ (charged particles, jet 2, in GeV) | - | - | - | 0.03 |
| $\cos(\delta\phi_{jets})$ | - | 0.67 | 0.94 | - |
| $p$ (highest momentum charged particle, in GeV/$c$) | -0.22 | - | - | - |
| $\langle E\rangle$ (neutral particles, in GeV) | -0.14 | - | - | - |

beam axis to be below 0.2 and 0.15, respectively, for the two selections.

For $\Delta M > 10$ GeV/$c^2$, at least 6 charged particles and a total energy in the range 25 to 100 GeV were required. The missing transverse momentum had to exceed 5 GeV/$c$. The missing momentum vector and the jet axes were required to be at more than 20° from the beam axis. Finally, the momentum of the most isolated (in angle) charged particle had to be below 20 GeV/$c$. Distributions of variables used in the initial selection are shown in Fig. 1 together with the expectations from Standard Model (SM) processes.

The final selection was optimised using a discriminating linear function [26]. For each squark, two functions were used per centre-of-mass energy, corresponding to the two domains of $\Delta M$. The functions were determined using training samples. Events were selected as candidates if they passed the selection for either one of the two mass domains. Efficiencies and backgrounds were then derived from statistically independent simulation data sets. A summary of the observables and coefficients used in constructing the functions for $\sqrt{s} = 161$ GeV can be found in Table 1. Similar values were found at $\sqrt{s} = 172$ GeV. The distributions of these functions for data, and the expected distributions for background and a typical signal, are shown in Fig. 2.

Table 2 summarises the results of the selection on data and simulated background samples. Note that most of the backgrounds for stop and sbottom are common to both channels. As a result, a high correlation exists in the remaining background in the sbottom and stop analyses. After applying the discriminating functions, no candidate event was selected in data.

For each energy and squark flavour, efficiencies have been evaluated using up to 35 simulated samples, each at a different point in the $(M_{\tilde{q}}, M_{\tilde{\chi}_1^0})$ plane covering squark

**Table 2.** Number of events selected in data and in background simulation for both flavours after combining the two $\Delta M$ domains. The rightmost column lists the main sources of background. Note that most of the backgrounds for stop and sbottom are common to both channels. The systematic error on the final background values was evaluated from differences in the distributions in data and simulation, as explained in the text

| **stop** | data | background simulation | background composition |
|---|---|---|---|
| $\sqrt{s} = 161$ GeV | 0 | $1.07 \pm 0.23(stat)\ ^{+0.29}_{-0.32}(sys)$ | 40% $q\bar{q}(\gamma)$, 18% $We\nu_e$ |
| $\sqrt{s} = 172$ GeV | 0 | $0.92 \pm 0.14(stat)\ ^{+0.37}_{-0.20}(sys)$ | 26% $ZZ$, 22% $q\bar{q}(\gamma)$ |
| **sbottom** | data | background simulation | background composition |
| $\sqrt{s} = 161$ GeV | 0 | $0.68 \pm 0.19(stat)\ ^{+0.10}_{-0.13}(sys)$ | 63% $q\bar{q}(\gamma)$, 18% $ZZ$ |
| $\sqrt{s} = 172$ GeV | 0 | $0.80 \pm 0.12(stat)\ ^{+0.18}_{-0.14}(sys)$ | 26% $ZZ$, 20% $q\bar{q}(\gamma)$ |

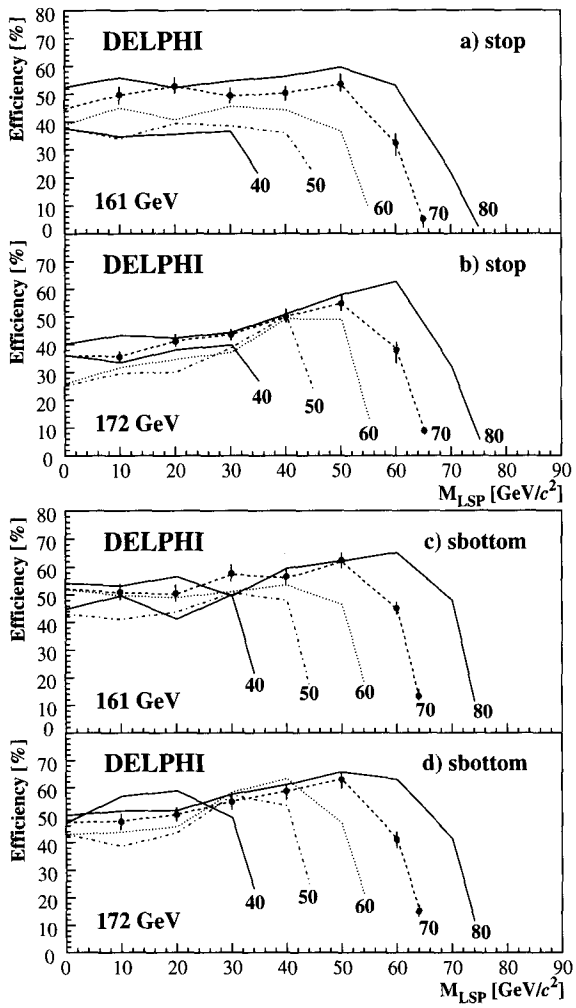


**Fig. 3.** Efficiencies for the stop **a,b** and sbottom **c,d** selections as a function of $M_{\tilde{\chi}^0_1}$, at centre-of-mass energies of 161 **a,c** and 172 GeV **b,d**. The curves correspond to different values of $M_{\tilde{q}}$, which are indicated on the plots in units of GeV/$c^2$. On the curves for $M_{\tilde{q}} = 70$ GeV, the simulated points and their combined statistical and systematic errors are shown. The maxima at $\Delta M = M_{\tilde{q}} - M_{LSP} \approx 20$ GeV/$c^2$ are due to the overlap of the selections for low and high $\Delta M$

masses between 40 and 80 GeV/$c^2$ and neutralino masses between 0 and 75 GeV/$c^2$. These efficiencies proved to be stable in the non-degenerate domain, and lower for smaller mass differences, as shown in Fig. 3. Systematic effects on efficiencies and backgrounds were estimated by moving all relevant distributions in the simulation by the difference between their mean values and the measured values found in the real data.

### 4.2 Exclusion limits in the $(M_{\tilde{q}}, M_{\tilde{\chi}^0_1})$ plane

Exclusion limits at 95% confidence level in the $(M_{\tilde{q}}, M_{\tilde{\chi}^0_1})$ plane are shown in Fig. 4. for several different assumptions on the nature of the lighter of the two squark states.

Since scalar mass unification suggests lower masses and cross-sections for the partners of right-handed fermions, an exclusion region for a pure $\tilde{b}_R$ is given ($\Theta_{mix} = 1.57$ rad), conservatively assuming the left-handed component to be kinematically inaccessible: for $\Delta M > 10$ GeV/$c^2$ a $\tilde{b}_R$ is excluded below 44 GeV/$c^2$. Conservative stop limits have been derived for the state with minimal cross-section ($\Theta_{mix} = 0.98$ rad), which corresponds approximately to a decoupling from the $Z^0$. For $\Delta M > 10$ GeV/$c^2$, the limit is 63 GeV/$c^2$.

Limits have also been calculated for pure left-handed components ($\Theta_{mix} = 0$), corresponding to the maximal cross-section. For mass differences $\Delta M$ to the LSP of more than 10 GeV/$c^2$, these limits are 72 GeV/$c^2$ for stop and 73 GeV/$c^2$ for sbottom.

## 5 Scalar lepton decay into neutralino and lepton

A signal in these channels is expected to give acoplanar leptons with missing momentum and energy. Here and elsewhere in this paper, 'acoplanar' is taken to mean acoplanar with the beam direction. Selections were applied both to simulated background and signal events and optimised to reduce the expected Standard Model background to about 1 event whilst keeping a reasonable efficiency for

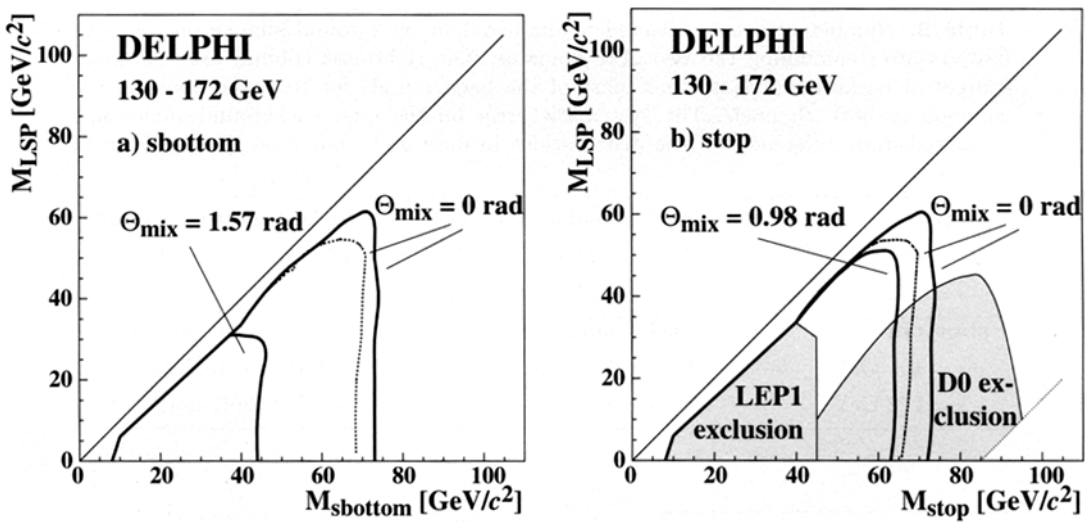


**Fig. 4.** Excluded regions at 95% C.L. in the $(M_{\tilde{q}}, M_{\tilde{\chi}_1^0})$ plane for **a** sbottom and **b** stop squarks. Combined limits from the runs above the $Z^0$-resonance are shown for $\tilde{q}_L$ ($\Theta_{mix} = 0$), corresponding to the maximal cross-section, and for the mixing angle which yields the minimal cross-section. The dotted curves indicate the mean limit for $\tilde{q}_L$ expected from background-only experiments. The observed limits are within the 95% probability zones of the expected limits. Regions already excluded at LEP1 [28] and by D0 [29] are shaded

the signal over a wide range of the slepton-neutralino mass difference.

### 5.1 Selection of selectrons and smuons

The selection of selectrons maximized the acceptance for electrons in the forward and backward regions of the detector. For events having less than ten charged particles, all the tracks in the forward and backward regions ($|\cos(\theta)| > 0.77$) which had an associated cluster in an electromagnetic calorimeter and had less than 10% of their associated calorimetric energy recorded in the hadronic calorimeter were considered as electron candidates. The electromagnetic energy not associated to a track but in a 3° cone around the track of the electron candidate was added to the electromagnetic energy of the candidate. The momentum of the electron candidate was then rescaled to match the electromagnetic energy.

After applying this procedure, events with exactly two well reconstructed, isolated charged particles with momentum above 1 GeV/$c$ and below 75% of the beam momentum were selected. There had to be no reconstructed clusters in the last 3 layers of the hadronic calorimeter associated to either particle (this acts as an efficient muon veto). Their invariant mass had to lie between 4 GeV/$c^2$ and 70 GeV/$c^2$ and their acoplanarity had to exceed 12°. If both particles were in the barrel region of the detector, at least one of them had to be classified as an electron using the standard DELPHI electron identification procedure [12] for $|\cos(\theta)| \leq 0.77$. The total multiplicity of the event had to be eight or smaller and the neutral energy less than 12 GeV. The missing energy of the event had to exceed 55 GeV and the transverse momentum of the pair of particles had to exceed 6 GeV/$c$. Events with an isolated signal in the taggers and missing momentum pointing towards it were rejected.

The selection of smuons required exactly two well reconstructed, isolated, oppositely charged particles with momenta above 1 GeV/$c$ and polar angles in the range $20° < \theta < 160°$. At least one of the particles was required to be loosely identified as a muon [13], and no more than 40% of the centre-of-mass energy should be associated with either particle. It was further required that the particle deposited less than 40% of its energy in the electromagnetic calorimeter if the momentum of the most energetic particle was between 33 and 47 GeV/$c$ (40 and 60 GeV/$c$) for 161 (172) GeV data. This cut reduces WW background. The total energy of particles in the forward and backward 30° cones had to be less than 30% of the visible energy, and the polar angle of the missing momentum had to lie between 20° and 160°.

In order to reject background from $e^+e^- \to q\bar{q}(\gamma)$ events and two-photon interactions, the total multiplicity of the event was required to be seven or smaller, the energy deposited in the small angle calorimeter STIC had to be less than 12 GeV and there should be no isolated neutral particle with energy larger than 10 GeV. The missing energy of the event had to exceed 30% of the centre-of-mass energy. The transverse momentum of the pair of particles was required to exceed 7 GeV/$c$. If the missing energy of the event was greater than 80% of the centre-of-mass energy, this requirement was relaxed to 5.5 GeV/$c$ and, in addition, the acoplanarity between the two selected tracks was required to be greater than 15°. If the missing energy of the event was less than 30% of the centre-of-mass energy, it was accepted if the acoplanarity was greater than 40° and the transverse momentum was

**Table 3.** Selectron and smuon candidates, together with the total number of background events expected and the conributions from the main background sources

| | 161 GeV | 172 GeV | 161 GeV | 172 GeV |
|---|---|---|---|---|
| Channel | $\tilde{e} \to e\tilde{\chi}_1^0$ | $\tilde{e} \to e\tilde{\chi}_1^0$ | $\tilde{\mu} \to \mu\tilde{\chi}_1^0$ | $\tilde{\mu} \to \mu\tilde{\chi}_1^0$ |
| Observed events | 1 | 0 | 1 | 0 |
| Total background | $1.7^{+0.8}_{-0.3}$ | $2.0^{+0.7}_{-0.2}$ | $0.5^{+0.2}_{-0.1}$ | $1.5^{+0.2}_{-0.1}$ |
| $Z^0/\gamma \to (\mu\mu,ee,\tau\tau)(n\gamma)$ | $0.4^{+0.3}_{-0.1}$ | $0.4^{+0.2}_{-0.1}$ | $0.1^{+0.1}_{-0.1}$ | $0.0^{+0.1}_{-0.0}$ |
| 4-fermion (except $\gamma\gamma$) | $1.1^{+0.7}_{-0.2}$ | $1.1^{+0.2}_{-0.1}$ | $0.4^{+0.1}_{-0.0}$ | $1.5^{+0.1}_{-0.0}$ |
| $\gamma\gamma \to \tau^+\tau^-$ | $0.1^{+0.2}_{-0.1}$ | $0.3^{+0.2}_{-0.1}$ | $0.0^{+0.1}_{-0.0}$ | $0.0^{+0.1}_{-0.0}$ |
| $\gamma\gamma \to ee, \mu\mu$ | $0.1^{+0.2}_{-0.1}$ | $0.2^{+0.6}_{-0.1}$ | $0.0^{+0.1}_{-0.0}$ | $0.0^{+0.1}_{-0.0}$ |

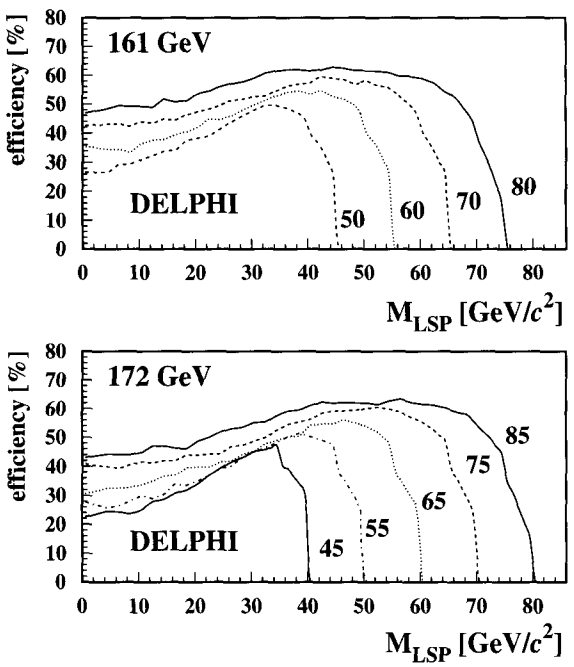


**Fig. 5.** Efficiencies for the selectron selection as a function of $M_{\tilde{\chi}_1^0}$, at centre-of-mass energies of 161 and 172 GeV. The curves correspond to different values of $M_{\tilde{e}}$ in units of GeV/$c^2$

greater then 25 GeV/$c$. The different requirements for high (low) missing energy were optimised for low (high) values of $\Delta M$=$M_{\tilde{\mu}}$-$M_{\tilde{\chi}_1^0}$. Events with an isolated signal in the taggers and with the missing momentum pointing towards it were rejected.

The selection efficiency of the search for selectrons and smuons was evaluated using fully simulated samples generated with SUSYGEN. The efficiencies for a subset of the fully simulated signal Monte Carlo used for selectrons are shown in Fig. 5. Uncertainties are typically in the range from 1.6 to 2.2%.

The efficiencies were then derived for the entire region of interest in 1 GeV/$c^2$ by 1 GeV/$c^2$ grids by interpolating the signal efficiencies in ($M_{\tilde{l}}$,$M_{\tilde{\chi}_1^0}$( space, evaluated using generator level Monte-Carlo events.

Table 3 summarises the numbers of accepted events in the data for the different selections and the numbers of events expected from the different background channels.

One candidate was found in the selectron channel. The event contains acoplanar particles with energies of 2.2 GeV and 23 GeV, the invariant mass of the pair of particles is 8.8 GeV/$c^2$, and the angle between particle directions is 34° in the plane perpendicular to the beam. The event is compatible with WW $\to \tau\tau\nu\nu$ or a Compton scattering process with a converted photon.

A candidate event was also found in the smuon channel. It consists of two well identified muons of 35 GeV/$c$ each and an invariant mass of 51 GeV/$c^2$. The transverse momentum of the muon pair is 19 GeV/$c$. The event is compatible with $WW \to \mu\mu\nu\nu$.

### 5.2 Selection of staus

To select events with a signature of two acoplanar taus with high missing energy, well reconstructed charged and neutral particles were grouped together: neutrals were associated to the closest charged particle. Groups were merged together if their invariant mass was below 5.5 GeV/$c^2$; if more than one such merging was possible, the one with the lowest mass was retained. This procedure was repeated until no more low-mass merged groups could be constructed. Comparison between data and simulation shows very good agreement, as can be seen in Fig. 6.

Events with exactly two such groups were considered as stau candidates if:

- the acoplanarity of the two groups was between 4° and 170°,
- the calorimetric energy in a 30° cone around the beam-axis did not exceed 10 GeV,
- the total number of reconstructed tracks was 6 or less,
- the energy of the most energetic, isolated photon was below 25 (18) GeV for centre-of-mass energies of 161 or 172 (130 or 136) GeV,
- the sum of the transverse momenta of all reconstructed charged particles was above 4 GeV/$c$,

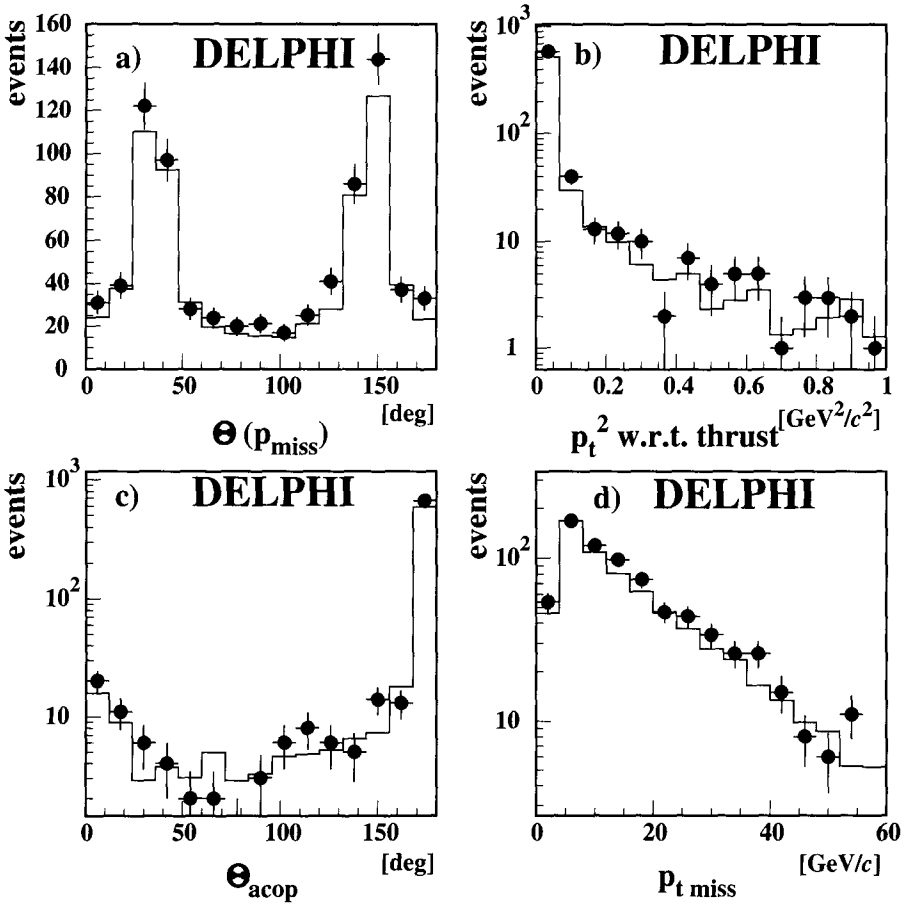


**Fig. 6.** A comparison of data and simulation in the stau analysis at 172 GeV centre-of-mass energy for all events after pre-selection into two groups of particles: distributions of **a** missing momentum polar angle, **b** transverse momentum squared of the particles with respect to the thrust axis, **c** acoplanarity and **d** missing transverse momentum. The dots with error bars represent the data while the simulation is shown by the solid line

- there were at least two charged particles with momentum above 1 GeV/$c$,
- the square of the transverse momentum with respect to the thrust axis was greater than 0.30 (GeV/$c$)$^2$, and
- the absolute value of the sum of the particle charges in the event was less than 2.

The events passing these selections were then sorted into four classes, according to which background channel dominated:

- "$Z/\gamma \to \mu^+\mu^-$" events had at least one particle with momentum above 60 GeV/$c$,
- "$\gamma\ \gamma$" events had no particle with momentum above 10 GeV/$c$,

otherwise events were classified by their acoplanarity:

- "$Z/\gamma \to \tau^+\tau^-$" events had acoplanarity less than 15°,
- "WW" events had acoplanarity greater than or equal to 15°.

The "$Z/\gamma \to \mu^+\mu^-$" class contains almost no signal events at the masses of interest for this analysis, and was not considered further.

To reduce the background in the "$\gamma\ \gamma$" class, the missing transverse momentum was required to exceed the larger of 6 GeV/$c$ or $(14-0.2\theta_{acop})$ GeV/$c$, where the acoplanarity, $\theta_{acop}$, is measured in degrees. (The latter condition removes events that simultaneously have low acoplanarity and transverse momentum.)

The background in the "$Z/\gamma \to \tau^+\tau^-$" class was reduced by noting that such events enter as candidates if an ISR photon was not detected, usually because it escaped down the beam-pipe. Since the reconstructed jets in such processes tend to be rather close in angle to the taus, the value of the available energy, $\sqrt{s'}$, can be calculated, assuming that a photon has escaped in the direction of the beam. Only events with values of $\sqrt{s'}$ less than 6 GeV below the centre-of-mass energy and not in the interval 81 to 96 GeV were retained. In addition, it was required that the missing momentum was at an angle greater than 30° to the beam.

Finally, in the "WW" class, the background taus tend to have larger momenta than those from the signal: while a W decaying into a tau and a neutrino is indistinguishable from a stau decaying into a tau and a low-mass neutralino, the two Ws need not decay into the same final state. Hence, demanding that the highest momentum particle in the event have momentum less than 40 GeV/$c$ left mainly those WW events where both Ws decay into tau, and therefore reduced this background to acceptable levels for centre-of-mass energies up to 161 GeV. At 172 GeV, this requirement had to be supplemented by a harder cut on the momentum of the more energetic lepton in the event: it was required to be less than 35 GeV/$c$. This class of events also contains a sizeable background from radiative return and $\gamma\gamma$ events with an ISR photon. To reduce contamination from these sources, it was also required

**Table 4.** Stau candidates, together with the total number of background events expected and the contributions from major background sources

| | 130 GeV | 136 GeV | 161 GeV | 172 GeV |
|---|---|---|---|---|
| Channel | $\tau \to \tau\tilde{\chi}_1^0$ | $\tau \to \tau\tilde{\chi}_1^0$ | $\tau \to \tau\tilde{\chi}_1^0$ | $\tau \to \tau\tilde{\chi}_1^0$ |
| Observed events | 1 | 0 | 1 | 0 |
| Total Background | $0.5^{+0.7}_{-0.3}$ | $0.5^{+0.4}_{-0.3}$ | $2.5^{+0.6}_{-0.3}$ | $2.5^{+0.7}_{-0.3}$ |
| $Z^0/\gamma \to (\mu\mu,ee,\tau\tau)(n\gamma)$ | $0.3^{+0.2}_{-0.1}$ | $0.2^{+0.2}_{-0.1}$ | $1.0 \pm 0.2$ | $0.5 \pm 0.1$ |
| 4-fermion (except $\gamma\gamma$) | $0.1 \pm 0.1$ | $0.2 \pm 0.1$ | $0.9 \pm 0.2$ | $1.9 \pm 0.2$ |
| $\gamma\gamma \to \tau^+\tau^-$ | $0.1^{+0.5}_{-0.0}$ | $0.1^{+0.2}_{-0.1}$ | $0.4^{+0.3}_{-0.1}$ | $0.1^{+0.2}_{-0.1}$ |
| $\gamma\gamma \to ee, \mu\mu$ | $0.0^{+0.3}_{-0.0}$ | $0.0^{+0.3}_{-0.0}$ | $0.2^{+0.5}_{-0.1}$ | $0.0^{+0.6}_{-0.0}$ |

that the missing momentum was at an angle of greater than 30° to the beam and, in the case where one electron was identified, that it was not at an angle of around 40° to the beam where the calorimetric coverage is incomplete.

These cuts selected two events, one at 130 GeV centre-of-mass energy, and one at 161 GeV. The candidate at 130 GeV consists of two well identified electrons of 32 and 40 GeV/$c$ each, with an invariant mass of 67 GeV/$c^2$. The one at 161 GeV consists of one loosely identified muon of 22 GeV/$c$ and a 15 GeV/$c$ hadron track and is compatible with a radiative return to the $Z^0$ with subsequent decay into a pair of taus.

Table 4 summarises the number of accepted events in the data and the expectations from the various background channels. Note that these backgrounds include those which were found while searching for selectrons and smuons. This should be accounted for when combining the three slepton channels.

As the total number of events seen in the data was low compared to the expected background, in particular at 172 GeV, the WW sample was studied in more detail. Three different event generators were used for this channel (EXCALIBUR, PYTHIA, and PYTHIA with tau-polarization taken into account). The background-level evaluated was compatible for all three samples. The candidate events for the process WW$\to$ $l\nu l\nu$ found in the DELPHI WW analysis were scrutinized. All were found to have been correctly rejected, either because of topology (3 events), or because of the visible mass (5 events).

In order to determine the efficiencies for the selection of staus, events were generated according to the MSSM, using SUSYGEN. The events generated were fed into two detector simulation programs, the full DELPHI simulation DELSIM, and a fast, simplified program. It was checked that the fast simulation results agree with the DELSIM results within the statistical errors. The fast simulation was then used to scan the entire region of interest in a 1 GeV/$c^2$ by 1 GeV/$c^2$ grid with 10000 events per point (72 million events). The efficiencies were found to be around 40 % in the entire plane (see Fig. 7), except at points where the difference between the stau and neutralino masses is small, where it falls to low values. Uncertainties were typically 1%.

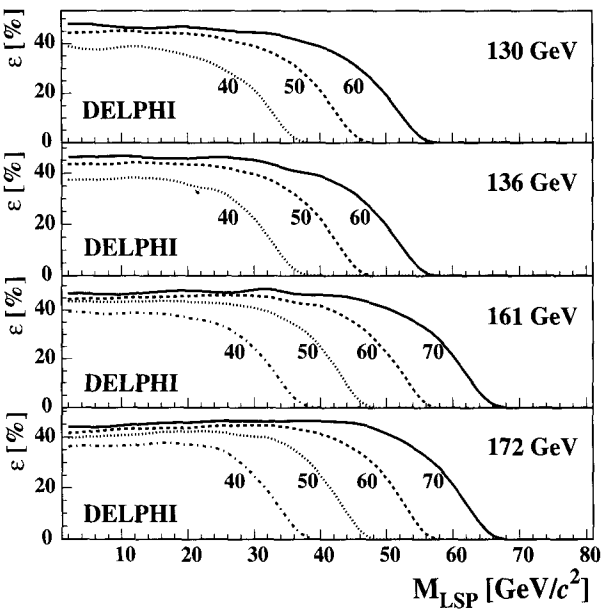


**Fig. 7.** Efficiencies for the stau selection as a function of $M_{\tilde{\chi}_1^0}$, at centre-of-mass energies of 130, 136, 161 and 172 GeV. The lines correspond to different values of $M_{\tilde{\tau}}$, which are indicated on the plots in units of GeV/$c^2$

### 5.3 Exclusion limits in the ($M_{\tilde{l}}$,$M_{\tilde{\chi}_1^0}$) plane

Exclusion limits for the production of selectrons and smuons were computed for $\tilde{e}_R\tilde{e}_R$ and $\tilde{\mu}_R\tilde{\mu}_R$ production, because in the MSSM the right-handed sleptons are expected to be lighter and to have lower production cross-sections than the corresponding left-handed sleptons, thus leading to the most conservative limits.

In the case of $\tilde{e}_R\tilde{e}_R$ production, limits were calculated for the deep gaugino region ($\mu = -200$ GeV/$c^2$). Figure 8a shows the 95% confidence level exclusion regions for $\tan\beta = 1.5$ and $\tan\beta = 35$, taking into account the candidate and the expected backgrounds in the regions of $M_{\tilde{e}}$ and $M_{\tilde{\chi}_1^0}$ with which they were kinematically compatible. Using these values for the MSSM parameters, a mass limit for $\tilde{e}_R$ can be set at 73.7 GeV/$c^2$ for $\tan\beta = 1.5$,

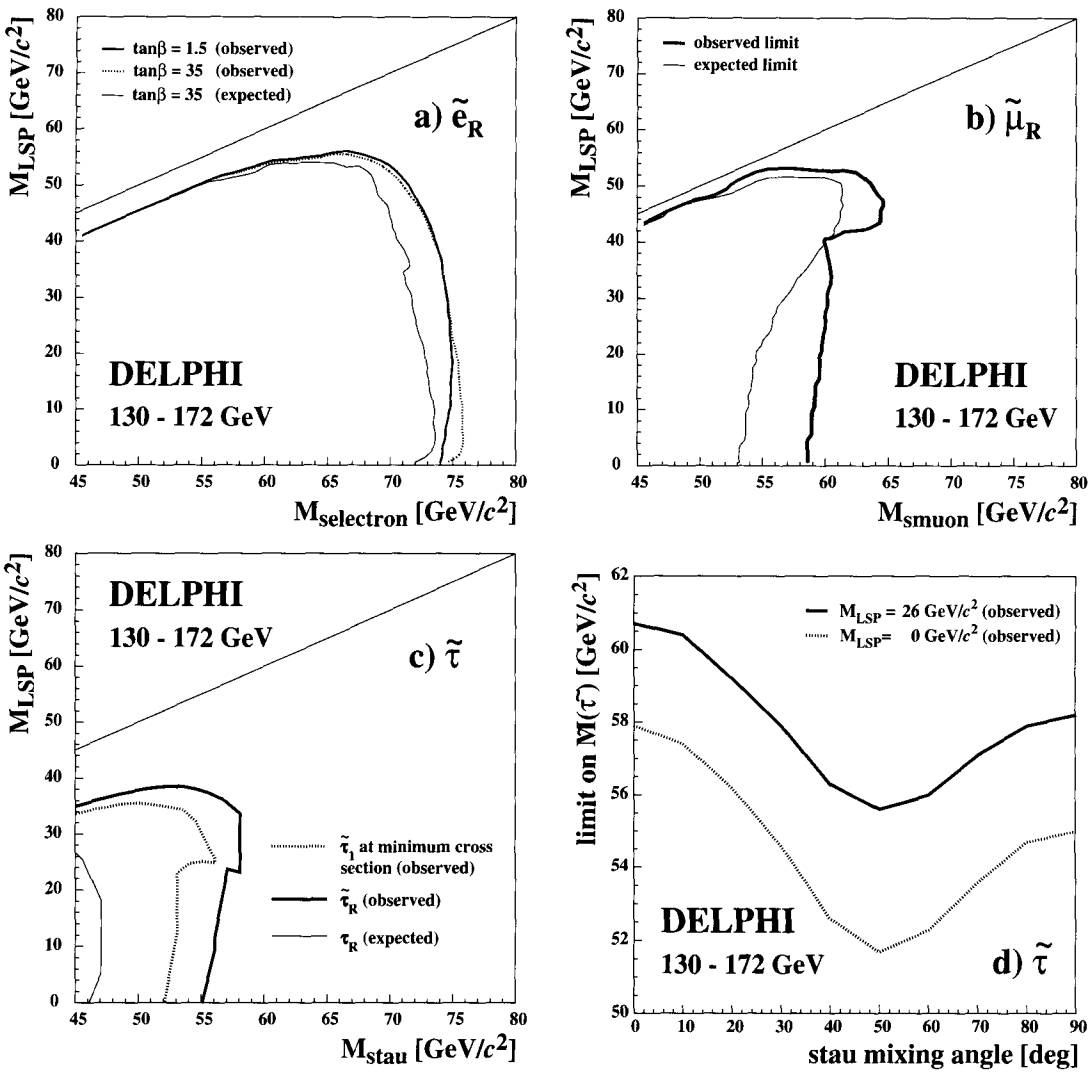


**Fig. 8.** 95% confidence level exclusion regions for **a** selectrons ($\tilde{e}_R$) for $\mu = -200$ and $\tan\beta = 1.5$ (solid curve) and 35 (dotted curve), **b** smuons ($\tilde{\mu}_R$, solid curve), **c** staus (the solid curve is for pure $\tilde{\tau}_R$, the dotted curve for the stau mixing angle yielding the lowest cross-section), **d** 95% CL mass limits for stau as a function of the mixing angle, for LSP masses of 26 GeV/$c^2$ (solid curve) and 0 GeV/$c^2$ (dotted curve). In plots **a**–**c** the additional thin curves indicate the mean limit expected from background-only experiments. The observed limits are in the 95% probability zones for these expected limits

if the LSP mass is below 40 GeV/$c^2$ and the selectron is heavier than 45 GeV/$c^2$.

For production of $\tilde{\mu}_R^+\tilde{\mu}_R^-$, Fig. 8b shows the excluded regions at 95% confidence level again assuming a kinematically inaccessible $\tilde{\mu}_L$, as suggested by the running of scalar mass terms in the MSSM. Here also, the candidate as well as the expected four-fermion background events were included in the range of $M_{\tilde{\mu}}$ and $M_{\tilde{\chi}_1^0}$ with which they were kinematically compatible. A mass limit of 58.6 GeV/$c^2$ for $\tilde{\mu}_R$ could be set for an LSP mass below 40 GeV/$c^2$ and smuon mass above 45 GeV/$c^2$.

The momentum of the visible particles produced by a stau decay follows a more complex distribution than the flat distribution present for selectron and smuon decays. In particular, there is no lower limit on the visible momentum. Hence, all candidates found both in the simulated background and in the experimental data must be considered as candidates at all points in the ($M_{\tilde{\tau}}$, $M_{\tilde{\chi}_1^0}$) plane that have $P_{seen}^{max} < P_{theor}^{max}(M_{\tilde{\tau}}, M_{\tilde{\chi}})$.

Combining the efficiency, the background-level and the number of candidates at each point in the stau-neutralino mass plane yields the 95 % likelihood regions shown in Fig. 8c. The figure shows the exclusion region for pure right stau and for the stau mixing angle yielding the lowest cross-section. A limit of 55 GeV/$c^2$ for the mass of the pure right stau is found for neutralino masses below 35 GeV/$c^2$ and stau masses above 45 GeV/$c^2$. Figure 8d shows the minimal allowed stau-mass as a function of the mixing-angle for an LSP mass of zero and for the LSP mass giving the highest stau mass limit.

As the observed mass limit, albeit high, was found to be within the 95 % confidence band of the expected limit, it is concluded that the low number of observed events is indeed a statistical fluctuation.

## 6 Slepton decays in the light gravitino scenario

In addition to the search for "standard" scalar leptons described above, a search for long lived scalar taus was performed. If the next to lightest supersymmetric particle is a slepton ($\tilde{l}$), its decay width to lepton and gravitino is given by the two-body equation [30]:

$$\Gamma(\tilde{l} \to l + \tilde{\mathrm{G}}) = \frac{m_{\tilde{l}}^5}{48\pi M_p^2 M_{\tilde{\mathrm{G}}}^2} \qquad (1)$$

where fermions have been considered massless and $M_p$ is the Planck mass. The mean decay length obtained from (1):

$$L = 1.76 \times 10^{-3}\ (E_{\tilde{l}}^2/m_{\tilde{l}}^2 - 1)^{\frac{1}{2}} \times \left(\frac{m_{\tilde{l}}}{100\,\mathrm{GeV}}\right)^{-5} \left(\frac{M_{\tilde{\mathrm{G}}}}{1\,\mathrm{eV}}\right)^2 \ cm \qquad (2)$$

depends strongly on the slepton mass ($m_{\tilde{l}}$) and the gravitino mass ($M_{\tilde{\mathrm{G}}}$). $E_{\tilde{l}}$ is the energy of the slepton.

A search has been made for $\tilde{l} \to l + \tilde{\mathrm{G}}$ decays within the detector volume, assuming that the $\tilde{l}$ (NLSP) is a right-handed $\tilde{\tau}$. The stau could be degenerate with other sleptons, which would then contribute to this search, but this analysis considers the most conservative hypothesis where they do not.

The signature of such an event will be a track with a kink or a decay vertex when the $\tilde{\tau}$ decays inside the tracking devices. If the decay length is too short (small $M_{\tilde{\mathrm{G}}}$) to allow the reconstruction of the $\tilde{\tau}$ track, only the decay products of the $\tau$ will be seen in the detector, and the search will then be based on track impact parameters. However, if the decay takes place outside the tracking devices (large $M_{\tilde{\mathrm{G}}}$), the signature will be that of a heavy charged particle already studied in DELPHI [31]. These searches have been combined to investigate a larger range of $\tilde{\mathrm{G}}$ masses.

### 6.1 Selection of long lived particles

The analysis was based on the full data sample collected by DELPHI during 1995 and 1996. Detection efficiencies were computed using 40000 simulated events generated at centre-of-mass energies of 133, 161 and 172 GeV with the $\tilde{\tau}$ mean decay length ranging from 0.25 cm to 1000 cm and $\tilde{\tau}$ masses from 45 GeV/$c^2$ to 80 GeV/$c^2$ and passed through the full DELPHI detector simulation. Trigger efficiencies were studied by simulating the DELPHI trigger response to the events selected, and were found to be around 99%.

#### 6.1.1 Search for secondary vertices

This analysis tried to exploit the peculiarity of the $\tilde{\tau} \to \tau\tilde{\mathrm{G}}$ topology, namely one or two tracks coming from the interaction point and at least one of them with either a secondary vertex or a kink. Reconstruction of secondary vertices is illustrated on Fig. 9, which shows a decay vertex and the variables used in the analysis.

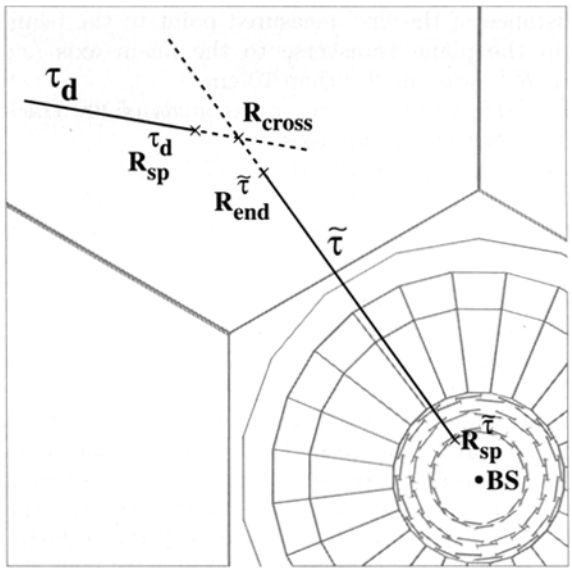


**Fig. 9.** Sketch of a decay vertex/kink in the plane perpendicular to the beam to illustrate its reconstruction. The stau track (full line labelled $\tilde{\tau}$) and the track of the decay product of the tau (full line labelled $\tau_d$) are extrapolated (dashed lines) to their crossing point ($R_{cross}$). $R_{sp}^{\tilde{\tau}}$ and $R_{end}^{\tilde{\tau}}$ are the first and last measured points of the $\tilde{\tau}$ track. $R_{sp}^{\tau_d}$ is the first measured point on the track selected as the $\tau$ decay product. All the distances are measured from the beam spot (BS)

Rather loose general requirements were first imposed on the events in order to suppress the low energy background:

- charged multiplicity between 2 and 10,
- visible energy above 10 GeV,
- sum of the transverse momenta with respect to the beam axis greater than 5 GeV/$c$,
- energy measured in the very forward calorimeters below 10 GeV,

leaving only about 4.7% of the whole data sample. The same conditions were applied at all the centre-of-mass energies. No quality requirements were imposed on the reconstructed tracks at this stage. Instead, the tracks were grouped into clusters according to their first measured point (starting point). This cluster procedure has been described in [32]. Each cluster contained all the tracks with distances between starting points less than 2 cm. The cluster starting point was defined as the average of the starting points of its tracks. The procedure allowed clusters with a single track if its momentum was larger than 1.5 GeV/$c$. The event was rejected if more than 6 tracks were not grouped into clusters or no cluster was found.

A cluster with only one track was considered as a $\tilde{\tau}$ candidate track if:

- the distance of the first measured point to the beam spot in the plane transverse to the beam axis ($xy$ plane), $R_{\tilde{\tau}}^{sp}$, was smaller than 10 cm,
- $|\cos\theta| < 0.8$, where $\theta$ is the polar angle of the track with respect to the beam axis,
- its momentum was greater than 2 GeV/$c$,
- its impact parameter along the beam axis and in the plane perpendicular to it were less than 10 and 5 cm, respectively.

For each $\tilde{\tau}$ candidate (single track cluster fulfilling the above conditions), a search was made for a second cluster with starting point in the $xy$ plane greater than $R_{\tilde{\tau}}^{sp}$, and an angular separation between the directions defined by the beam spot and the cluster starting points smaller than 90° in the $xy$ plane. This second cluster was assumed to be formed by the decay products of the $\tau$ coming from the $\tilde{\tau} \rightarrow \tau\tilde{G}$ process. Therefore, the $\tilde{\tau}$ candidate and the $\tau$ cluster had to define a secondary vertex. If the $\tau$ cluster included more than one track, only the track with the highest momentum was used to search for the decay vertex or kink (crossing point with the $\tilde{\tau}$ track).

The tracks were parametrized with respect to their perigee [33] to calculate the point of closest approach between the two tracks (the candidate $\tilde{\tau}$ track and the selected track from the $\tau$ cluster candidate). The following conditions were required to define a good crossing point:

- the minimum distance between the tracks had to be below 1 mm in the $xy$ plane,
- the crossing point, the end point of the stau track, and the start point of the tau daughter were required to satisfy the following conditions:

$$-10\,cm < (R_{cross} - R_{end}^{\tilde{\tau}}) < 25\,cm$$
$$-25\,cm < (R_{cross} - R_{sp}^{\tau}) < 10\,cm$$

where $R_{end}^{\tilde{\tau}}$, $R_{cross}$ and $R_{sp}^{\tau}$ are the distance of the end point of the $\tilde{\tau}$ track, the crossing point of the tracks and the starting point of the $\tau$ daughter track from the beam spot in the $xy$ plane.

Fake secondary vertices could be produced by particles interacting in the detector material, or by radiated photons if the particle trajectory was reconstructed in two separate track segments. To eliminate this kind of event, additional requirements were imposed:

- any hadronic interaction had to be outside a 5° cone around the kink direction to reject hadronic interactions in the detector walls,
- if the $\tau$ cluster had only one track, no neutral particle could be present in a 1° cone around the direction defined by the difference between the $\tilde{\tau}$ momentum and the momentum of the $\tau$ daughter, to reject photon radiation,
- if it had more tracks, the angle between the momenta of the tracks used to define a vertex, calculated at the crossing point, had to exceed 2° to reject segmented tracks.

If no pair of tracks was found to fulfil these conditions, the event was rejected.

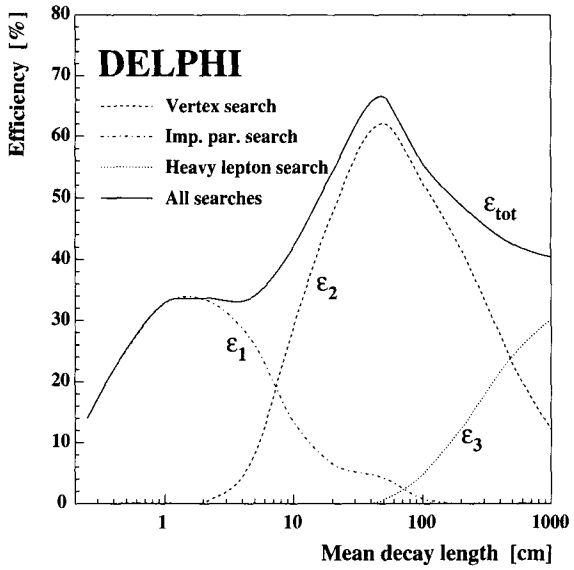


**Fig. 10.** Efficiency of the impact parameter search ($\varepsilon_1$), vertex search ($\varepsilon_2$), heavy lepton search ($\varepsilon_3$) [31] and total efficiency ($\varepsilon_{tot}$) for a $\tilde{\tau}$ of 60 GeV/$c^2$at a centre-of-mass energy of 172 GeV

The efficiencies for different mean decay lengths, $\tilde{\tau}$ masses and centre-of-mass energies were calculated by applying the above selections to the simulated signal samples. Figure 10 shows the efficiencies ($\varepsilon_2$) obtained for a 60 GeV/$c^2$ $\tilde{\tau}$ at a centre-of-mass energy of 172 GeV and for decay lengths from 0.25 to 1000 cm. The vertex reconstruction efficiency was sensitive to the decay length in the $xy$ plane (R). Between 15 cm and 90 cm it was ~75% since the VD and the ID were needed to reconstruct the $\tilde{\tau}$ track. It dropped to zero for $\tilde{\tau}$s decaying near the outer edge of the TPC.

The selection efficiency was about 94% inside the sensitive region, but it had to be scaled by the fraction of $\tilde{\tau}$ decays within this volume which, for a mean decay length of 50 cm, was about 65%. The shape of the efficiency distribution remained the same, independent of the $\tilde{\tau}$ mass and of the centre-of-mass energy; it simply scaled down near the kinematic limit. The loss of efficiency near the kinematic limit was due to the fact that the $\tilde{\tau}$ boost was smaller and the kink reconstruction less efficient when the angles between the $\tilde{\tau}$ and the $\tau$ products increased.

### 6.1.2 Impact parameter search

To investigate the region of low gravitino masses (short decay lengths) the previous search was extended to the case of the $\tilde{\tau}$ decaying between 0.25 cm and around 10 cm. In this case the $\tilde{\tau}$ track was not reconstructed in the ID and only the $\tau$ decay products were detected. The signature for this topology was two tracks with large impact parameters and large acollinearities. Cosmic rays, badly reconstructed tracks or interactions in the detector material could result in large impact parameters. However, the

**Table 5.** The number of events observed, together with the total number of background events expected and the numbers expected from the individual background sources

| | 172 GeV | 161 GeV | 130-136 GeV |
|---|---|---|---|
| Channel: | $\tilde{\tau} \to \tau\tilde{G}$ | $\tilde{\tau} \to \tau\tilde{G}$ | $\tilde{\tau} \to \tau\tilde{G}$ |
| Observed events | 0 | 0 | 0 |
| Total background | $0.44^{+0.19}_{-0.13}$ | $0.36^{+0.16}_{-0.10}$ | $0.04^{+0.64}_{-0.03}$ |
| $Z^0/\gamma \to (\tau\tau)(n\gamma)$ | $0.07^{+0.06}_{-0.04}$ | $0.14^{+0.07}_{-0.05}$ | $0.04^{+0.05}_{-0.03}$ |
| $Z^0/\gamma \to (ee)(n\gamma)$ | $0.17^{+0.14}_{-0.09}$ | $0.13^{+0.05}_{-0.04}$ | $0.00^{+0.21}_{-0.00}$ |
| 4-fermion (except $\gamma\gamma$) | $0.04^{+0.02}_{-0.02}$ | $0.00^{+0.02}_{-0.00}$ | $0.00^{+0.04}_{-0.00}$ |
| $\gamma\gamma \to \tau^+\tau^-$ | $0.16^{+0.12}_{-0.09}$ | $0.09^{+0.13}_{-0.08}$ | $0.00^{+0.60}_{-0.00}$ |

two tracks in a cosmic event usually had impact parameters of the same order and opposite sign. The acollinearity in events with badly reconstructed tracks or interactions was always small.

The impact parameter search was applied only to those events accepted by the general cuts, described previously, but not selected by the secondary vertex analysis. The events were accepted as candidates if:

- there were two single track clusters in the event (i.e. two tracks with momentum larger than 1.5 GeV/$c$ and a distance between starting points larger than 2 cm),
- the first measured point of at least one of the tracks was within 12 cm of the beam axis,
- both tracks were reconstructed in the TPC to guarantee a good track reconstruction,
- at least one of the tracks had an impact parameter larger than 0.2 cm in the plane transverse to the beam axis, to remove standard events,
- the ratio of the impact parameters of the two tracks was smaller than 1.5 and larger than -0.5, to reject cosmic rays,
- the acollinearity between the two tracks was larger than 10°.

The efficiencies were derived for the different $\tilde{\tau}$ masses, decay lengths and centre-of-mass energies by applying the same selection to the simulated signal events. Figure 10 shows the efficiency of the impact parameter search ($\varepsilon_1$) for a 60 GeV/$c^2$ $\tilde{\tau}$ at a centre-of-mass energy of 172 GeV. The maximum efficiency was 33.5%, corresponding to a mean decay length of 2 cm. It decreased very fast for lower decay lengths due to the cut on minimum impact parameter. For longer decay lengths the efficiency decreased smoothly due to the cut on the maximum number of tracks, because in this situation the $\tilde{\tau}$ track could be reconstructed. The losses of efficiency for $\tilde{\tau}$ masses near the kinematic limit and due to initial state radiation were also considered.

An independent analysis aiming at even shorter $\tilde{\tau}$ lifetimes was also performed. In that case the background from standard model processes becomes larger. Tighter preselection cuts were then adopted in order to allow a looser impact parameter cut. Comparable results were obtained [34].

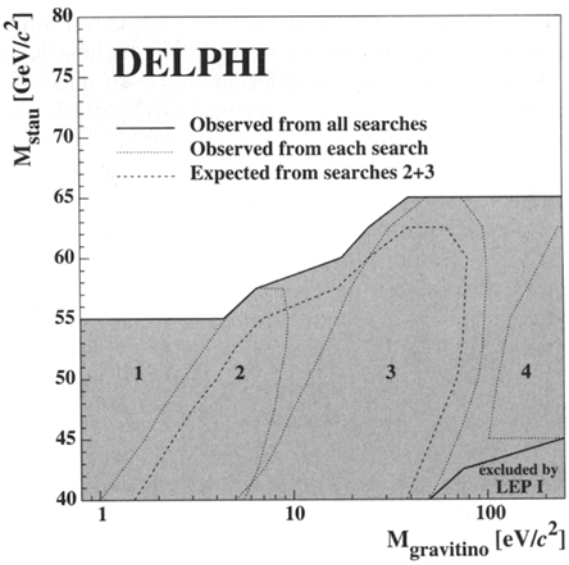


**Fig. 11.** Exclusion region in the ($M_{\tilde{\tau}}$,$M_{\tilde{G}}$) plane at 95% CL for the present analysis combined with the stable heavy lepton search and the results of Sect. 5.2. The region covered by the LEP I searches for stable heavy leptons is also shown. The dotted lines show the exclusion regions from each search: (1) from the analysis of Sect. 5.2, (2) from the impact parameter search, (3) from the vertex search, and (4) from the stable heavy lepton search. The dashed line indicates the mean limit expected from background-only experiments for the combination of impact parameter and vertex searches

### 6.2 Exclusion limits in the ($M_{\tilde{\tau}}$,$M_{\tilde{G}}$) plane

No events were found in the data. The total numbers of background events expected are shown in Table 5.

The result of the above analyses was combined with that of the stable heavy lepton search described in [31], which considered the $\tilde{\tau}$ decays outside the tracking devices ($R > 200$ cm) and covered slepton masses from 45 GeV/$c^2$ to the kinematic limit. Figure 10 shows the efficiency of the stable heavy lepton search ($\varepsilon_3$) for a stau mass of 60 GeV/$c^2$ at a centre-of-mass energy of 172 GeV as a function of the decay length. For large $\tilde{\tau}$ masses, efficiencies around 70% were obtained. Also shown is the combined efficiency of the three analyses ($\varepsilon_{tot}$). As an event could be selected by the vertex search and by the stable heavy lepton search, the correlation was taken into account.

Upper limits at 95% CL on the production of $\tilde{\tau}$ were calculated for the different centre-of-mass energies. Upper limits around 0.6 pb were obtained for $M_{\tilde{G}} > 8$ eV/$c^2$ at 172 GeV and for $M_{\tilde{G}} > 10$ eV/$c^2$ at 161 GeV centre-of-mass energy. Due to the lower luminosity at 133 GeV, only an upper limit on the production cross-section of 1 pb was set for $M_{\tilde{G}} > 10$ eV/$c^2$.

Since no candidates were observed, the expected number of events was computed to exclude $m_{\tilde{\tau}}$ values as a function of $M_{\tilde{G}}$, combining the different centre-of-mass energies and all the analyses. The vertex search allows the exclusion, at 95% CL, of $\tilde{\tau}$ masses around 60 GeV/$c^2$ in the range of intermediate gravitino masses (25 to 100 eV/$c^2$). The stable heavy lepton search covers the high gravitino mass region (over 100 eV/$c^2$). The impact parameter analysis covers the region of low gravitino masses.

Combining these results with the results of Sect. 5.2 from $\tilde{\tau}_R$ decays into $\tau$ and neutralino allow the exclusion of stau masses, at 95% CL, below 55 GeV/$c^2$ irrespective of the gravitino mass. The results are shown in Fig. 11.

## 7 Conclusions

In a data sample of 21 pb$^{-1}$ collected by the DELPHI detector at centre-of-mass energies of 161 and 172 GeV, searches were performed for events with acoplanar lepton or jet pairs. The results were combined with those already obtained between 130 and 136 GeV and substantially extend the exclusion limits obtained at LEP1. All limits were computed at the 95% confidence level.

No candidate was found in the search for scalar partners of heavy quarks in the decay modes $\tilde{t} \to c\tilde{\chi}_1^0$ and $\tilde{b} \to b\tilde{\chi}_1^0$, excluding pure $\tilde{t}_L$ ($\tilde{b}_L$) squarks below 72 (73) GeV/$c^2$ respectively, for $\Delta M = M_{\tilde{q}} - M_{\tilde{\chi}_1^0} > 10$ GeV/$c^2$. In the same $\Delta M$ region, a stop at minimal cross-section is excluded below 63 GeV/$c^2$, whereas the limit for a pure $\tilde{b}_R$ is found to be 44 GeV/$c^2$.

One candidate was found in the selectron channel, compatible with the background expectation. For $\mu = -200$ GeV/$c^2$ a mass limit for $\tilde{e}_R$ can be set at 73.7 GeV/$c^2$ (73.5 GeV/$c^2$) for $\tan\beta = 1.5$ (35), if the LSP mass is below 40 GeV/$c^2$. In the search for smuon production one event was selected. For right-handed scalar muons a limit of 58.6GeV/$c^2$is obtained if the LSP mass is below 40 GeV/$c^2$. The search for stau decays into tau and neutralino gave two candidates. A mass limit of 55 GeV/$c^2$ was found for the $\tilde{\tau}_R$ if the neutralino mass is below 35 GeV /$c^2$. These limits apply for slepton masses higher than 45 GeV/$c^2$.

Combined with the above result, the search for stau decays in the light gravitino scenario excludes stau masses below 55 GeV/$c^2$ irrespective of the mass of the gravitino.

*Acknowledgements.* We are greatly indebted to our technical collaborators, to the members of the CERN-SL Division for the excellent performance of the LEP collider, and to the funding agencies for their support in building and operating the DELPHI detector. We acknowledge in particular the support of Austrian Federal Ministry of Science and Traffics, GZ 616.364/ 2-III/2a/98, FNRS-FWO, Belgium, FINEP, CNPq, CAPES, FUJB and FAPERJ, Brazil, Czech Ministry of Industry and Trade, GA CR 202/96/0450 and GA AVCR A1010521, Danish Natural Research Council, Commission of the European Communities (DG XII), Direction des Sciences de la Matière, CEA, France, Bundesministerium für Bildung, Wissenschaft, Forschung und Technologie, Germany, General Secretariat for Research and Technology, Greece, National Science Foundation (NWO) and Foundation for Research on Matter (FOM), The Netherlands, Norwegian Research Council, State Committee for Scientific Research, Poland, 2P03B06015, 2P03B03311 and SPUB/ P03/178/98, JNICT–Junta Nacional de Investigação Cientifica e Tecnológica, Portugal, Vedecka grantova agentura MS SR, Slovakia, Nr. 95/5195/134, Ministry of Science and Technology of the Republic of Slovenia, CICYT, Spain, AEN96–1661 and AEN96-1681, The Swedish Natural Science Research Council, Particle Physics and Astronomy Research Council, UK, Department of Energy, USA, DE–FG02–94ER40817.

## References

1. P. Fayet, S. Ferrara, Phys. Rep. **32**, 249 (1977); H.P. Nilles, Phys. Rep. **110**, 1 (1984); H.E. Haber, G.L. Kane, Phys. Rep. **117**, 75 (1985)
2. DELPHI Collaboration: P. Abreu et al., Phys. Lett. B **387**, 651 (1996)
3. ALEPH Collaboration: R. Barate et al., Phys. Lett. B **413**, 431 (1997); ALEPH Collaboration: R. Barate et al., Phys. Lett. B **407**, 377 (1997); L3 Collaboration: M. Acciarri et al., E. Phys. J. C **4**, 207 (1998); L3 Collaboration: M. Acciarri et al., Phys. Lett. B **377**, 289 (1996); OPAL Collaboration: K. Ackerstaff et al., Z. Phys. C **75**, 409 (1997); OPAL Collaboration: K. Ackerstaff et al., Phys. Lett. B **396**, 301 (1997)
4. M. Drees, K. Hikasa, Phys. Lett. B **252**, 127 (1990); J. Ellis, S. Rudaz, Phys. Lett. B **128**, 248 (1983)
5. DELPHI Collaboration: P. Abreu et al., E. Phys. J. C **1**, 1 (1998)
6. ALEPH Collaboration: R. Barate et al., E. Phys. J. C **2**, 3 (1998); L3 Collaboration: M. Acciarri et al., E. Phys. J. C **4**, 207 (1998); OPAL Collaboration: K. Ackerstaff et al., E. Phys. J. C **2**, 213 (1998)
7. M. Dine, W. Fischler, M. Srednicki, Nucl. Phys. B **189**, 575 (1981); M. Dine, W. Fischler, Phys. Lett. B **110**, 227 (1982); M. Dine, M. Srednicki, Nucl. Phys. B **202**, 238 (1982); L. Alvarez Gaumé, M. Claudson, M. Wise, Nucl. Phys. B **207**, 96 (1982); C. Nappi, B. Ovrut, Phys. Lett. B **113**, 175 (1982)
8. M. Dine, W. Fischler, Nucl. Phys. B **204**, 346 (1982); S. Dimopoulos, S. Raby, Nucl. Phys. B **219**, 479 (1983)
9. S. Dimopoulos, M. Dine, S. Raby, S. Thomas, J.D. Wells, Nucl. Phys. Proc. Suppl. **52A**, 38 (1997)
10. S. Dimopoulos, M. Dine, S. Raby, S. Thomas, Phys. Rev. Lett. **76**, 3494 (1996)
11. S. Dimopoulos, S. Thomas, D. Wells, Phys. Rev. D **54**, 3283 (1996)
12. DELPHI Collaboration: P. Abreu et al., Nucl. Instr. and Meth. A **303**, 233 (1991)
13. DELPHI Collaboration: P. Abreu et al., Nucl. Instr. and Meth. A **378**, 57 (1996)
14. P. Rebecchi, "*Optimisation de l'herméticité du détecteur DELPHI pour la recherche de particules supersymétriques à LEP2* ", Ph.D. thesis, LAL 96-30, Université Paris XI Orsay
15. T. Sjöstrand, Comp. Phys. Comm. **82**, 74 (1994); T. Sjöstrand, "*High energy physics event generation with* PYTHIA 5.7, JETSET 7.4", CERN TH/7111-93 (1993, rev. 1994)

16. DELPHI Collaboration: P. Abreu et al., Z. Phys. C **73**, 11 (1996)
17. S.Katsanevas, S.Melachroinos in "*Physics at LEP2* ", CERN 96-01, Vol.2, p.328
18. S. Ambrosanio, B. Mele, Phys. Rev. D **52**, 3900 (1995); S. Ambrosanio, B. Mele, Phys. Rev. D **53**, 2451 (1996)
19. S. Kawabata, Comp. Phys. Comm. **41**, 127 (1986)
20. W. Beenakker, R. Hopker, M. Spira, P.M. Zerwas, Phys. Lett. B **349**, 463 (1995)
21. F.A. Berends, R. Pittau, R. Kleiss, Comp. Phys. Comm. **85**, 437 (1995)
22. S. Nova, A. Olshevski, T. Todorov, "*A Monte Carlo event generator for two photon physics*", DELPHI note 90-35 PROG 152
23. F.A. Berends, P.H. Daverveldt, R. Kleiss, Monte Carlo Simulation of Two-Photon Processes, Comp. Phys. Comm. **40**, 271 (1986)
24. A.L. Read, "*Optimal statistical analysis of search results based on the likelihood ratio and its application to the search for the MSM Higgs boson at* $\sqrt{s}$ *= 161 and 172 GeV*", DELPHI note 97-158 PHYS 737
25. S. Bethke et al., Phys. Lett. B **213**, 235 (1988)
26. R.A. Fisher, "*The use of multiple measurements in taxonomic problems*", Annals of Eugenics, **7** (1936)
27. G.C. Fox, S. Wolfram, Nucl. Phys. B **149**, 413 (1979)
28. OPAL Collaboration: R. Akers et al., Phys. Lett. B **337**, 207 (1994)
29. D0 Collaboration: S. Abachi et al., Phys. Rev. Lett. **76**, 2222 (1996)
30. S. Ambrosanio, G.L. Kane, G.D. Kribs, S.P. Martin, S. Mrenna, Phys. Rev. D **54**, 5395 (1996)
31. DELPHI collaboration: P. Abreu et al., Phys. Lett. B **396**, 315 (1997)
32. DELPHI collaboration: P. Abreu et al., Z. Phys. C **74**, 57 (1997)
33. P. Billoir, S. Qian, Nucl. Instr. and Meth. A **311**, 139 (1992)
34. C. Lacasta, C. Garcia, R. Alemany, F. Cavallo, F.L. Navarria, "*Preliminary search for long-lived* $\tilde{\tau}$ *using the DELPHI detector*", DELPHI note 97-97 CONF-99, submitted to HEP'97, Jerusalem, Aug 19-26, 1997